Thermodynamic Modeling and Optimum Design Strategy of a Generic Solid Oxide Fuel Cell–Based Hybrid System

ARTICLE *in* ENERGY & FUELS · JULY 2012

Impact Factor: 2.79 · DOI: 10.1021/ef300839m

3 AUTHORS, INCLUDING:

Jincan Chen
Xiamen University
325 PUBLICATIONS **4,108** CITATIONS

energy&fuels

Article

pubs.acs.org/EF

Thermodynamic Modeling and Optimum Design Strategy of a Generic Solid Oxide Fuel Cell-Based Hybrid System

Xiuqin Zhang, Juncheng Guo, and Jincan Chen*

Department of Physics, Xiamen University, Xiamen 361005, People's Republic of China

ABSTRACT: A generic model of the hybrid system mainly consisting of a solid oxide fuel cell (SOFC) and a heat engine is established, in which some main irreversibilities existing in real hybrid systems are considered. On the basis of the developed models of the SOFC and Brayton cycle with a regenerative process, analytical expressions for the power outputs and efficiencies of the subsystems and hybrid system are derived. It is found that for given parameters, the maximum power density of the hybrid system may attain 3.24 times of that of a single SOFC. Moreover, the general performance characteristics of the hybrid system are revealed and the optimal criteria of some of the main operating parameters are determined. The influence of the regenerative process in the heat engine is discussed in detail. It shows that through the introduction of a regenerator in the heat engine, the maximum power output of the hybrid system under the ideal regenerative condition will increase 51.51%. It is important to note that the results obtained here may be directly used to reveal the general performance characteristics of some special interesting hybrid systems consisting of a SOFC and a gas turbine or a Carnot heat engine.

I. INTRODUCTION

The increased worldwide demand for electrical power requires high fuel-to-electricity conversion efficiencies even in small-scale power plants. The hybrid power plant of a solid oxide fuel cell (SOFC) and a gas turbine (GT) can reach this goal and have efficiency over 60% for small power outputs (200−400 kW).[1−4] The perspective of full commercialization of the SOFC−GT hybrid plants is very attractive because of the small gas turbines which have entered the marketplace, and the performance of small-capacity SOFC−GT, SOFC−MGT, full, and partial load SOFC−GT hybrid systems have been investigated widely.[5−8]

In the development of SOFC−GT hybrid technologies, both modeling and simulation play an important role. Some control strategies, including the least-squares support vector machine, Lagrange multipliers, and so on, have been employed to control the optimized power output, fuel and air flows, temperature, and fuel utilization of the hybrid systems.[9−15] The comparative performance analyses of the hybrid power plants fuelled with methane, methanol, ethanol, and dimethyl-ether (DME) have been carried out for the performance improvement of hybrid systems.[16]

The integration strategies for the SOFC and gas turbine consist of direct thermal coupling, indirect thermal coupling, or fuel coupling.[5,17,18] Here, we consider an indirectly combined system of a SOFC and a generic heat engine cycle, which is different from the coupling of high temperature fuel cells with Carnot heat engines, indirectly coupled solid oxide fuel cell/gas turbine hybrid power plants, or integration of a SOFC with a Stirling engine,[19−23] because it can be used to expound the general performance characteristics of a SOFC-based hybrid system, investigate the key irreversible losses of the hybrid system, and obtain the optimum criteria of the main performance parameters.

In the present paper, the concrete contents are organized as follows. In section 2, a generic model of the hybrid system composed of a SOFC and a heat engine is established. The performance of the SOFC and heat engine with a regenerative process is briefly described. The power output and efficiency of the hybrid system are derived. In section 3, the general performance characteristics of the hybrid system are discussed and the optimal operating regions of some of the main performance parameters are determined. In section 4, some special cases are discussed in detail. The performance characteristics of several hybrid systems are directly revealed. Finally, some important conclusions are summarized.

2. MODEL DESCRIPTION OF A SOFC−HEAT ENGINE HYBRID SYSTEM

We consider a generic hybrid system mainly consisting of a SOFC and a heat engine, as shown in Figure 1, where the total electrochemical reaction of the SOFC is:

$$2H^+ + O^{2-} \rightarrow H_2O + \text{heat} + \text{electricity}$$

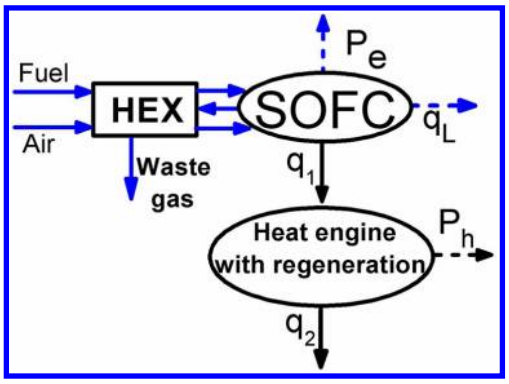

Figure 1. Schematic diagram of a SOFC−heat engine hybrid system.

Received: May 16, 2012
Revised: July 6, 2012
Published: July 9, 2012

dx.doi.org/10.1021/ef300839m | *Energy Fuels* 2012, 26, 5177−5185

The high-temperature waste heat produced in the SOFC is utilized as the heat input of heat engine, the waste gases generated in the SOFC are used to preheat the fuel and air through a heat exchanger, P_e and P_h are the power outputs of the SOFC and heat engine, respectively, q_1 and q_2 are the rates of heat flow from the SOFC at temperature T to the working air of the heat engine and from the working air of the heat engine to the environment at temperature T_O, respectively, and q_L is the heat leak rate from the SOFC to the environment. By using such a hybrid system, the waste heat produced in the SOFC can be instantly used and the performance of hybrid system will be improved.

2.1. Power Output and Efficiency of a SOFC. The electrochemical reaction in a SOFC is often assumed ideal and the fuel on the anode is totally reacted, but some irreversible losses which originate primarily from the activation overpotential (V_{act}), ohmic overpotential (V_{ohm}), and concentration overpotential (V_{con}) are always present in a SOFC.[24−28] Considering the influence of these irreversible losses on the performance of a SOFC in detail, one can derive the power output and efficiency of the SOFC as[19,29,30]

$$\begin{aligned} P_e &= iA_c(E - V_{act} - V_{ohm} - V_{con}) \\ &= \frac{iA_cRT}{n_eF}\left[\frac{-\Delta g(T)}{RT} + \ln\left(\frac{p_{H_2}p_{O_2}^{1/2}}{p_{H_2O}}\right)\right. \\ &\quad - 2\sinh^{-1}\left(\frac{i}{2i_{0,a}}\right) - 2\sinh^{-1}\left(\frac{i}{2i_{0,c}}\right) + \ln\left(1 - \frac{i}{i_{L,a}}\right) \\ &\quad \left. + \ln\left(1 - \frac{i}{i_{L,c}}\right) - \frac{in_eFL_{el}}{\sigma_0 R}\exp\left(\frac{E_{el}}{RT}\right)\right] \end{aligned} \quad (1)$$

and

$$\begin{aligned} \eta_e &= \frac{P_e}{-\Delta\dot{H}} \\ &= \frac{-RT}{\Delta h(T)}\left[\frac{-\Delta g(T)}{RT} + \ln\left(\frac{p_{H_2}p_{O_2}^{1/2}}{p_{H_2O}}\right)\right. \\ &\quad - 2\sinh^{-1}\left(\frac{i}{2i_{0,a}}\right) - 2\sinh^{-1}\left(\frac{i}{2i_{0,c}}\right) \\ &\quad \left. + \ln\left(1 - \frac{i}{i_{L,a}}\right) + \ln\left(1 - \frac{i}{i_{L,c}}\right) - \frac{in_eFL_{el}}{\sigma_0 R}\exp\left(\frac{E_{el}}{RT}\right)\right] \end{aligned} \quad (2)$$

respectively, where $E = (RT/n_eF)[(-\Delta g(T)/RT) + \ln(p_{H_2}p_{O_2}^{1/2}/p_{H_2O})]$, $-\Delta\dot{H} = -iA_c\Delta h(T)/n_eF$, $\Delta g(T)$ and $\Delta h(T)$ are the molar Gibbs free energy change and enthalpy change of the species at temperature T and pressure $p_0 = 1$ atm, i is the current density, $i_{0,a}$ and $i_{0,c}$ are the anode and cathode exchange current densities, $i_{L,a}$ and $i_{L,c}$ are the limiting current densities of the anode and cathode, A_c is the surface area of the interconnect plate, n_e is the number of electrons transferred in reaction, F is Faraday's constant, R is the universal gas constant, p_{H_2}, p_{O_2}, and p_{H_2O} are, respectively, the partial pressures of reactants H_2, O_2, and H_2O, L_{el} is the thickness of electrolyte, E_{el} is the activation energy for ion transport, and σ_0 is the reference ionic conductivity.

2.2. Efficiency of a Heat Engine. The working substance cycle of the heat engine in the hybrid system can be modeled as a Brayton cycle with a regenerative process and its temperature−entropy diagram is shown in Figure 2, where 1−2S and 4−5S are

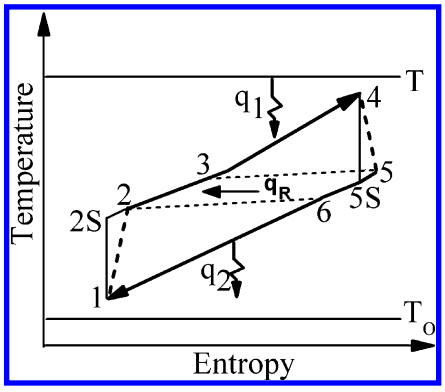

Figure 2. Temperature−entropy diagram of an irreversible Brayton cycle.

two reversible adiabatic processes, 1−2 and 4−5 are two irreversible adiabatic processes, 2S−4 and 5−1 are two isobaric processes, q_R is the rate of heat flow in the regenerator, and T_i (i = 1, 2, 3, 4, 5, 6) are the temperatures of the working substance at state points i.

To discuss the influence of irreversible losses in the Brayton cycle on the performance of hybrid system, the compression, expansion, and regeneration efficiencies of the Brayton cycle are usually introduced as[31−33]

$$\delta_c = \frac{T_{2S} - T_1}{T_2 - T_1} \quad (3)$$

$$\delta_e = \frac{T_4 - T_5}{T_4 - T_{5S}} \quad (4)$$

and

$$\delta_r = \frac{T_3 - T_2}{T_5 - T_2} \quad (5)$$

respectively. According to the property of reversible adiabatic processes in the Brayton cycle, one has

$$\frac{T_{2S}}{T_1} = \frac{T_4}{T_{5S}} = r_p^{1-1/\gamma} \quad (6)$$

where r_p is the pressure ratio of two isobaric processes 2S−4 and 5−1, and γ is the ratio of the specific heats of the working substance.

It is often assumed that the heat transfer between the working substance and heat reservoirs obeys the Newtonian law,[34,35] so the rates of heat flow of the three heat exchange processes in the Brayton cycle can be expressed as

$$q_1 = \dot{m}c_p(T_4 - T_3) = \frac{K_HA_H(T_4 - T_3)}{\ln[(T - T_3)/(T - T_4)]} \quad (7)$$

$$q_2 = \dot{m}c_p(T_6 - T_1) = \frac{K_LA_L(T_6 - T_1)}{\ln[(T_6 - T_O)/(T_1 - T_O)]} \quad (8)$$

and

dx.doi.org/10.1021/ef300839m | Energy Fuels 2012, 26, 5177−5185

$$q_R = \dot{m}c_p(T_3 - T_2) = \dot{m}c_p(T_5 - T_6) = K_R A_R(T_5 - T_3) = K_R A_R(T_6 - T_2) \quad (9)$$

respectively, where $\dot{m}$ and c_p are the mass flow rate and specific heat at constant pressure of the working substance in the cycle, respectively, K_H, K_L, and K_R are the heat transfer coefficients in isobaric processes 3−4 and 6−1 and regenerative process 5−6, respectively, A_H, A_L, and A_R are the corresponding heat transfer areas, and $A = A_H + A_L + A_R$ is the total heat transfer area of the heat engine. Combining eqs 3−9, one can rewrite the rate of heat flow from SOFC to heat engine as

$$q_1 = AK_H[T_4(1 - Y\delta_r) + T_1X(\delta_r - 1)] \Big/ \left[\ln\frac{T + T_1X(\delta_r - 1) - T_4Y\delta_r}{T - T_4} + \frac{K_H\delta_r}{K_R(1 - \delta_r)} + \frac{K_H}{K_L}\ln\frac{T_1X\delta_r + T_4Y(1 - \delta_r) - T_O}{T_1 - T_O}\right] \quad (10)$$

and obtain the efficiency of the heat engine as

$$\eta_h = 1 - \frac{q_2}{q_1} = 1 - \frac{T_4Y(1 - \delta_r) + T_1(X\delta_r - 1)}{T_4(1 - Y\delta_r) + T_1X(\delta_r - 1)} \quad (11)$$

where $X = 1 + (r_p^{1-1/\gamma} - 1)/\delta_c$ and $Y = 1 + (r_p^{1/\gamma-1} - 1)\delta_e$.

It can be proved that when the parameters r_p, T_1, and T_4 are determined by the following equations

$$\frac{TZ_1}{(T - T_4)Z_2} + \frac{K_H}{K_L}\frac{T_O[T_1(1 - X\delta_r) - T_4Y(1 - \delta_r)]}{(T_1 - T_O)Z_3} = \ln\frac{Z_2}{T - T_4} + \frac{K_H\delta_r}{K_R(1 - \delta_r)} + \frac{K_H}{K_L}\ln\frac{Z_3}{T_1 - T_O} \quad (12)$$

$$T_1[XY(\delta_r - 1)^2 - (1 - Y\delta_r)(1 - X\delta_r)] \Big/ \left\{1 - Y\delta_r - Z_1\left[\frac{1}{T - T_4} - \frac{Y\delta_r}{Z_2} + \frac{K_H}{K_L}\frac{Y(1 - \delta_r)}{Z_3}\right] \Big/ \left[\ln\frac{Z_2}{T - T_4} + \frac{K_H\delta_r}{K_R(1 - \delta_r)} + \frac{K_H}{K_L}\ln\frac{Z_3}{T_1 - T_O}\right]\right\} = \{[T_4(\delta_r - 1) + T_1(\delta_r + X - 2X\delta_r)]T_4\delta_e r_p^{1/\gamma-2} + [T_4(\delta_r + Y - 2\delta_rY) + T_1(\delta_r - 1)]T_1r_p^{-1/\gamma}/\delta_c\} \Big/ \left\{Z_4 + Z_1\left[\frac{-Z_4}{Z_2} + \frac{K_H}{K_L}\frac{T_1\delta_r r_p^{-1/\gamma}/\delta_c - T_4\delta_e(1 - \delta_r)r_p^{1/\gamma-2}}{Z_3}\right] \Big/ \left[\ln\frac{Z_2}{T - T_4} + \frac{K_H\delta_r}{K_R(1 - \delta_r)} + \frac{K_H}{K_L}\ln\frac{Z_3}{T_1 - T_O}\right]\right\} \quad (13)$$

and eq 10, the efficiency of the heat engine attains its optimum value for a given q_1, where $Z_1 = T_4(1 - Y\delta_r) + T_1X(\delta_r - 1)$, $Z_2 = T - T_4Y\delta_r + T_1X(\delta_r - 1)$, $Z_3 = T_4Y(1 - \delta_r) + T_1X\delta_r - T_O$, and $Z_4 = T_1(1 - \delta_r)r_p^{-1/\gamma}/\delta_c - T_4\delta_r\delta_e r_p^{1/\gamma-2}$.

Equations 10, 12, and 13 show that when the parameters K_H/K_R, K_H/K_L, T, T_O, δ_e, δ_c, δ_r, and γ are given, the optimum values $r_{p,\eta}$, $T_{1,\eta}$, and $T_{4,\eta}$ of the parameters r_p, T_1, and T_4 are only functions of $q_1/(AK_H)$. Substituting $r_{p,\eta}$, $T_{1,\eta}$, and $T_{4,\eta}$ into eq 11, one can obtain the optimum efficiency $\eta_{h,opt}$ of the heat engine, which is only a function of $q_1/(AK_H)$ for other given parameters.

2.3. Power Output and Efficiency of a Hybrid System.

As illustrated in Figure 1, one part of the waste heat produced in the fuel cell is directly released to the environment as heat leak q_L, and the other part is transferred to the heat engine in the hybrid system. The heat leak may be expressed as[36−39]

$$q_L = K_lA_l(T - T_O) \quad (14)$$

where K_l is the convective and/or conductive heat leak coefficient and A_l is the effective heat transfer area. According to the first law of thermodynamics and Figure.1, the rate of heat input from the SOFC to the heat engine can be derived as

$$q_1 = -\Delta\dot{H} - P_e - q_L \quad (15)$$

Combining eqs 2, 14, and 15, one can obtain

$$\frac{q_1}{AK_H} = a_1[(1 - \eta_e)i - a_2(T - T_O)] \quad (16)$$

where $a_1 = -(A_c\Delta h/n_eFAK_H)$ and $a_2 = -(K_lA_ln_eF/A_c\Delta h)$ and substituting eq 16 into eq 10 yields

$$a_1[(1 - \eta_e)i - a_2(T - T_O)] = Z_1/\left[\ln\frac{Z_2}{T - T_4} + \frac{K_H\delta_r}{K_R(1 - \delta_r)} + \frac{K_H}{K_L}\ln\frac{Z_3}{T_1 - T_O}\right] \quad (17)$$

.Using eqs 2, 12, 13, and 17, we can generate the curves of $r_{p,\eta}$, $T_{1,\eta}$, and $T_{4,\eta}$ versus current density i of the SOFC, as shown in Figures 3, 4, and 5, respectively. When the current density is

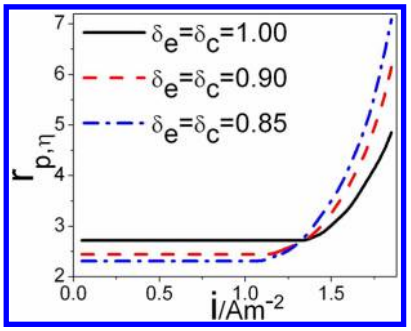

Figure 3. Curves of the pressure ratio $r_{p,\eta}$ versus current density for the parameters T = 1273 K, T_O = 300 K, $K_H = K_L = K_R$, δ_r = 0.95, γ = 1.4, a_1 = 0.001, and a_2 = 0.01.

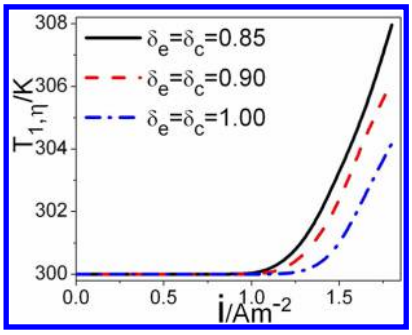

Figure 4. Curves of $T_{1,\eta}$ versus current density. The values of the parameters are the same as those used in Figure 3.

dx.doi.org/10.1021/ef300839m | Energy Fuels 2012, 26, 5177−5185

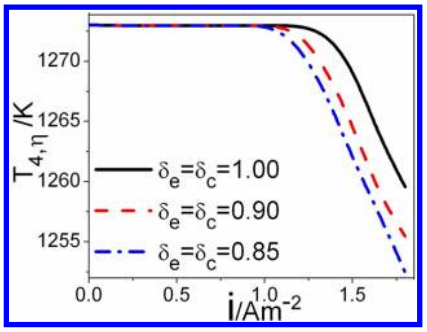

Figure 5. Curves of $T_{4,\eta}$ versus current density. The values of the parameters are the same as those used in Figure 3.

small, $r_{p,\eta}$ approaches to a constant, and $T_{1,\eta}$ and $T_{4,\eta}$ approach to T_O and T, respectively. When the current density is increased, the efficiency of the fuel cell decreases. When the current density is larger than around 1.0 A m^{-2}, not only the efficiency but also the power output of the fuel cell decreases, and consequently, the waste heat produced in the fuel cell increases quickly. In order to efficiently use the waste heat, $(T - T_{4,\eta})$ and $(T_{1,\eta} - T_O)$ are required to increase with the increasing of the current density. In such a case, $(T_{4,\eta} - T_{1,\eta})$ decreases rapidly. In order to improve the performance of the heat engine, $r_{p,\eta}$ has to be increased quickly. When the current density is increased to the maximum which is about 1.8 A m^{-2}, both the efficiency and power output of the fuel cell are equal to zero, as shown in Figures 6 and 7.

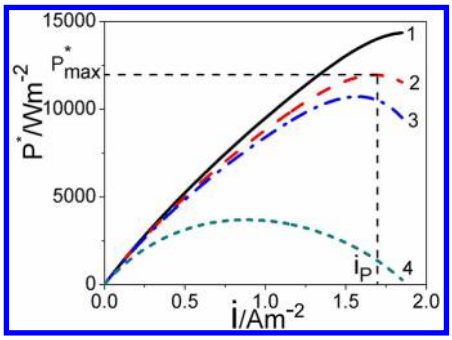

Figure 6. Power density versus current density curves, where i_P is the current density at the maximum power density P^*_{max} of the hybrid system. Curves 1−3 are the i−P^* curves of hybrid system corresponding to the cases in which (1) $\delta_e = \delta_c = 1.00$, (2) $\delta_e = \delta_c = 0.90$, and (3) $\delta_e = \delta_c = 0.85$, respectively. Curve 4 is the i−P^*_e curve of the SOFC. The values of the other parameters are the same as those used in Figure 3.

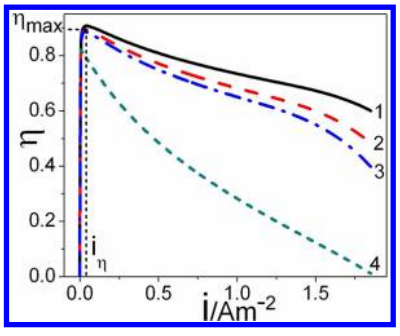

Figure 7. Efficiency versus current density curves, where i_η is the current density at the maximum efficiency η_{max}. Curves 1−3 are the i−η curves of the hybrid system and curve 4 is the i−η_e curve of the SOFC. The values of the parameters are the same as those used in Figure 6.

Combining eqs 2, 11, and 16, one can derive the power output and efficiency of the hybrid system as

$$P = P_e + q_1\eta_{h,opt} = -\frac{A_c\Delta h}{n_eF}\left\{i\eta_e + \left[1 - \frac{T_4Y(1-\delta_r) + T_1(X\delta_r - 1)}{T_4(1 - Y\delta_r) + T_1X(\delta_r - 1)}\right] \times [(1-\eta_e)i - a_2(T - T_O)]\right\} \quad (18)$$

and

$$\eta = \frac{P}{-\Delta\dot{H}} = \eta_e + \left[1 - \frac{T_4Y(1-\delta_r) + T_1(X\delta_r - 1)}{T_4(1 - Y\delta_r) + T_1X(\delta_r - 1)}\right] \times \left[1 - \eta_e - \frac{a_2}{i}(T - T_O)\right] \quad (19)$$

respectively. Using eqs 18 and 19, we can study the performance characteristics of the hybrid system numerically, obtain the optimally working regions of some of the important parameters, discuss the influence of the main irreversible losses on the performance of hybrid system, reveal the performance characteristics of the hybrid system under several interesting cases, and provide some theoretical bases for the optimum design and operation of practical SOFC-based hybrid systems.

3. GENERAL PERFORMANCE CHARACTERISTICS AND OPTIMUM CRITERIA

Below, numerical calculations are carried out based on the parameters summarized in Table 1, which are derived from the data available in the literature.[27,40−44] These parameters are kept constant unless mentioned specifically otherwise.

Table 1. Parameters used in the Model of an SOFC

parameter	value
operating pressure, p_0 (atm)	1
fuel composition pressures: p_{H_2}; p_{H_2O} (atm)	0.97; 0.03
air composition pressures: p_{O_2}; p_{N_2} (atm)	0.21; 0.79
number of electrons, n_e	2
electrolyte thickness, L_{el} (μm)	20
activation energy of O^{2-}, E_{el} (J mol^{-1})	8.0 × 10^4
prefactor of O^{2-}, σ_0 (S m^{-1})	3.6 × 10^7
molar enthalpy change at T = 1273 K, Δh (kJ mol^{-1})	−249.5
molar Gibbs free energy change at T = 1273 K, Δg (kJ mol^{-1})	−177.5
anode exchange current density, $i_{o,a}$ (A m^{-2})	1.261 × 10^3
cathode exchange current density, $i_{o,c}$ (A m^{-2})	5.644 × 10^3
anode limiting current density, $i_{L,a}$ (A m^{-2})	2.99 × 10^4
cathode limiting current density, $i_{L,c}$ (A m^{-2})	2.16 × 10^4
Faraday constant, F (C mol^{-1})	96 485
universal gas constant, R (J mol^{-1} K^{-1})	8.314

Using eqs 2, 12, 13, and 17−19, one can obtain the curves of the power density and efficiency of the hybrid system versus current density, as shown in Figures 6 and 7, respectively, where $P^* = P/A_c$ is the power density. It is seen from Figures 6 and 7 that the performance of the hybrid system is better than that of a SOFC and can be improved by increasing the compression and expansion efficiencies of the heat engine. It is

dx.doi.org/10.1021/ef300839m | Energy Fuels 2012, 26, 5177−5185

also seen from Figures 6 and 7 that there are a maximum power density and efficiency, with the corresponding current densities i_P and i_η, respectively. The maximum power density of the hybrid system may attain 3.24 times of that of a single SOFC, which is just between the results 1.24 and 4.64 obtained from the experiment and simulation.[6,10,45,46] In the region of $i < i_\eta$, both the power density and efficiency of hybrid system will decease as the current density decreases. In the region of $i > i_P$, both the power density and efficiency of hybrid system will decrease as the current density increases. It shows that the optimally operating region of the hybrid system should be situated in the region of $i_\eta \le i \le i_P$. When the hybrid system is operated in the region, the power density of the hybrid system will increase as the efficiency is decreases, and vice versa, as shown by curves 1−3 in Figure 8, where P^*_η and η_P are the

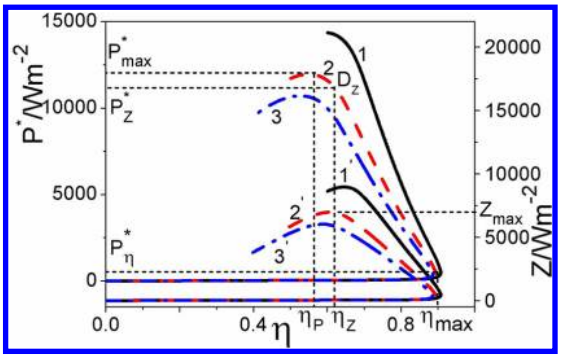

Figure 8. P^* and Z versus η curves of the hybrid system. Curves 1−3 are the $\eta-P^*$curves and curves 1′−3′ are the $\eta-Z$ curves corresponding to curves 1−3. Z_{max} is the maximum value of Z. η_P and η_Z are the efficiencies at P^*_{max} and Z_{max}, respectively. P^*_η and P^*_Z are the power densities at η_{max} and Z_{max}, respectively. The values of the parameters are the same as those used in Figure 6.

power density at the maximum efficiency and efficiency at the maximum power density, respectively. Obviously, the optimum regions of the power density and efficiency of the hybrid system should be $P^*_{max} \ge P^* \ge P^*_\eta$ and $\eta_p \le \eta \le \eta_{max}$ respectively. Thus, i_η and i_P, P^*_η and P^*_{max}, and η_P and η_{max} are the important parameters of the hybrid system, because they determine the lower bounds and upper bounds of the optimized values of the current density, power density, and efficiency, respectively.

It should be pointed out that, in general, a practical SOFC−heat engine hybrid system is not designed to operate at the state of the maximum efficiency because its corresponding power output is very small compared with the maximum power output. Thus, how to further give consideration to both power output and efficiency in the optimal region of $i_\eta \le i \le i_P$ becomes an important problem for the practical optimum design and operation of a SOFC−heat engine system. For this purpose, one may usually adopt some new objective functions, such as the ecological efficiency which evaluates the environmental impacts caused by the power plant emissions,[47−49] the energy cost used to obtain the most cost-effective performance of the system,[19] or other multiobjective functions,[37,50,51] to further discuss the optimal performance of the system. Here, we introduce the product of the efficiency and power density, i.e., $Z = \eta P^*$, as a new objective function and generate the $\eta-Z$ curves, as shown by curves 1′−3′ in Figure 8, where η_Z and P^*_Z are the efficiency and power density at the maximum value Z_{max} of Z, respectively. It is clearly seen from Figure 8 that point D_Z on the $\eta-P^*$ curve just corresponds to the state that the product of η and P^* attains its maximum and there exists the following relation: $Z_{max} = \eta_Z P^*_Z > \eta_P P^*_{max} > \eta_{max} P^*_\eta$. It shows that it is very significant to choose Z as an objective function. In general, one always wants to obtain a large power output and efficiency for a practical SOFC−heat engine hybrid system, and consequently, the power density and efficiency of the hybrid system should be chosen in the region of $P^*_Z \le P^* \le P^*_{max}$ and $\eta_Z \ge \eta \ge \eta_P$, respectively.

4. DISCUSSION

4.1. Influence of the Regenerative Process in the Heat Engine. If the regenerator in the heat engine is assumed to be ideal, $\delta_r = 1$ and $K_R \to \infty$. In such a case, the power output and efficiency of the hybrid system

$$P = -\frac{A_c \Delta h}{n_e F}\left\{ i\eta_e + \left[1 - \frac{T_{1,\eta}(X-1)}{T_{4,\eta}(1-Y)}\right]\left[(1-\eta_e)i - a_2(T - T_O)\right]\right\} \tag{20}$$

and

$$\eta = \eta_e + \left[1 - \frac{T_{1,\eta}(X-1)}{T_{4,\eta}(1-Y)}\right]\left[1 - \eta_e - \frac{a_2}{i}(T - T_O)\right] \tag{21}$$

can be directly derived from eqs 18 and 19, respectively. Equations 10 and 11 can be simplified as

$$q_1 = AK_H T_4(1-Y)\Big/\left(\ln\frac{T - T_4 Y}{T - T_4} + \frac{K_H}{K_L}\ln\frac{T_1 X - T_O}{T_1 - T_O}\right) \tag{22}$$

and

$$\eta_h = 1 - \frac{T_1(X-1)}{T_4(1-Y)} \tag{23}$$

respectively, where $A = A_H + A_L$. Using eqs 22 and 23 and the similar method mentioned above, one can determine the parameters $r_{p,\eta}$, $T_{1,\eta}$, and $T_{4,\eta}$ in eqs 20 and 21 and then generate the curves of the power density varying with efficiency of the hybrid system, as shown by curves 1 and 2 in Figure 9.

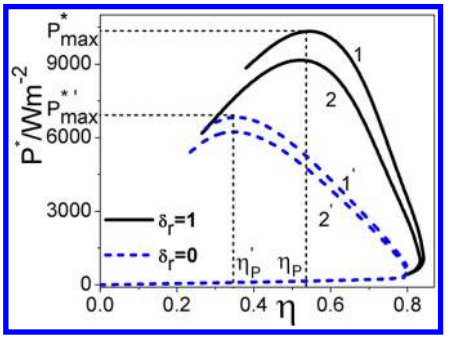

Figure 9. P^* versus η curves of the hybrid system under different irreversible conditions of the heat engine, where $r_p = 4.13$, $a_1 = 0.008$, and $a_2 = 0.08$. Curves 1 and 1′ correspond to the case of $\delta_e = \delta_c = 0.90$ and Curves 2 and 2′ correspond to the case of $\delta_e = \delta_c = 0.85$. The values of the other parameters are the same as those used in Figure 3.

dx.doi.org/10.1021/ef300839m | Energy Fuels 2012, 26, 5177−5185

If there does not exist a regenerator in the heat engine, q_R is directly released to the environment. In such a case, $\delta_r = K_R = 0$ and the power output and efficiency of the hybrid system

$$P = -\frac{A_c \Delta h}{n_e F}\left\{ i\eta_e + \left(1 - \frac{T_{4,\eta}Y - T_{1,\eta}}{T_{4,\eta} - T_{1,\eta}X}\right)[(1-\eta_e)i - a_2(T - T_O)]\right\} \quad (24)$$

and

$$\eta = \eta_e + \left(1 - \frac{T_{4,\eta}Y - T_{1,\eta}}{T_{4,\eta} - T_{1,\eta}X}\right)\left[1 - \eta_e - \frac{a_2}{i}(T - T_O)\right] \quad (25)$$

can be directly derived from eqs 18 and 19, respectively. Equations 10 and 11 can be simplified as

$$q_1 = AK_H(T_4 - T_1X)/\left[\ln\frac{T - T_1X}{T - T_4} + \frac{K_H}{K_L}\ln\frac{T_4Y - T_O}{T_1 - T_O}\right] \quad (26)$$

and

$$\eta_h = 1 - \frac{T_4Y - T_1}{T_4 - T_1X} \quad (27)$$

respectively, where $A = A_H + A_L$. The parameters $r_{p,\eta}$, $T_{1,\eta}$, and $T_{4,\eta}$ in eqs 24 and 25 can be determined by using the similar method mentioned above. Equations 24 and 25 can be used to plot the curves of the power density varying with efficiency of the hybrid system, as shown by curves 1′ and 2′ in Figure 9.

It is seen from curves 1 and 1′ in Figure 9 that the maximum power density of the hybrid system under the ideal regeneration condition will increase 51.51% compared with that of the hybrid system without the regenerative process in the heat engine. This shows clearly that the introduction of a regenerator in the heat engine can effectively improve the performance of the hybrid system.

If there is a regenerator in the heat engine while the regenerative process is nonideal, the power output and efficiency of the hybrid system are, respectively, given by eqs 18 and 19 and the curves of the power density varying with the efficiency of the hybrid system are shown by curves 1−3 in Figure 8.

4.2. Case of $T_1 = T_O$. If $T_1 = T_O$, the model established above will be equivalent to a SOFC−gas turbine (GT) hybrid system[6,7,52] shown in Figure 10, and consequently, we can directly derive the power output and efficiency of such a hybrid system

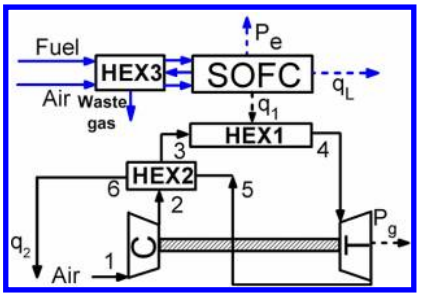

Figure 10. Schematic diagram of a SOFC−GT hybrid system.

$$P = -\frac{A_c \Delta h}{n_e F}\left\{ i\eta_e + \left[1 - \frac{T_{4,\eta}Y(1-\delta_r) + T_O(X\delta_r - 1)}{T_{4,\eta}(1 - Y\delta_r) + T_OX(\delta_r - 1)}\right][(1-\eta_e)i - a_2(T - T_O)]\right\} \quad (28)$$

and

$$\eta = \eta_e + \left[1 - \frac{T_{4,\eta}Y(1-\delta_r) + T_O(X\delta_r - 1)}{T_{4,\eta}(1 - Y\delta_r) + T_OX(\delta_r - 1)}\right]\left[1 - \eta_e - \frac{a_2}{i}(T - T_O)\right] \quad (29)$$

from eqs 18 and 19, respectively. Equations 10 and 11 can be simplified as

$$q_1 = AK_H[T_4(1 - Y\delta_r) + T_OX(\delta_r - 1)]/\left[\ln\frac{T + T_OX(\delta_r - 1) - T_4Y\delta_r}{T - T_4} + \frac{K_H\delta_r}{K_R(1-\delta_r)}\right] \quad (30)$$

and

$$\eta_h = 1 - \frac{T_4Y(1-\delta_r) + T_O(X\delta_r - 1)}{T_4(1 - Y\delta_r) + T_OX(\delta_r - 1)} \quad (31)$$

respectively, where $A = A_H + A_R$ because the working substance cycle in the GT may be modeled as an open Brayton cycle.[53−55] Parameters $r_{p,\eta}$ and $T_{4,\eta}$ in eqs 28 and 29 can be obtained by using the similar method mentioned above. The performance characteristic curves of the SOFC−GT hybrid system are shown by curve 4 in Figures 11 and 12.

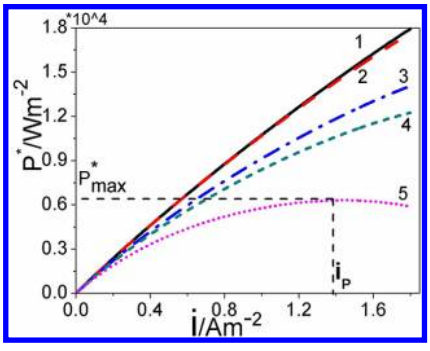

Figure 11. P^* versus i curves of the hybrid system under different irreversible conditions of the heat engine where $\delta_e = \delta_c = 0.90$. Curves 3, 4, and 5 correspond to the cases in which $\delta_r = 1$, $\delta_r = 0.9$, and $\delta_r = 0$, respectively. The values of the other parameters are the same as those used in Figure 3.

When the regenerator in GT is assumed to be ideal, $K_R \to \infty$, $\delta_r = 1$, and the power output and efficiency of the hybrid system

$$P = -\frac{A_c \Delta h}{n_e F}\left\{ i\eta_e + \left[1 - \frac{T_O(X-1)}{T_{4,\eta}(1-Y)}\right][(1-\eta_e)i - a_2(T - T_O)]\right\} \quad (32)$$

dx.doi.org/10.1021/ef300839m | Energy Fuels 2012, 26, 5177−5185

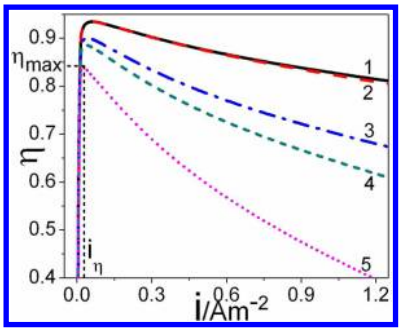

Figure 12. η versus i curves of the hybrid system under different irreversible conditions of the heat engine. The values of the parameters are the same as those used in Figure 11.

and

$$\eta = \eta_e + \left[1 - \frac{T_O(X-1)}{T_{4,\eta}(1-Y)}\right]\left[1 - \eta_e - \frac{a_2}{i}(T - T_O)\right] \tag{33}$$

can be obtained from eqs 28 and 29, respectively. Equations 30 and 31 can be simplified as

$$q_1 = A_H K_H T_4 (1-Y)/\ln\left(\frac{T - T_4 Y}{T - T_4}\right) \tag{34}$$

and

$$\eta_h = 1 - \frac{T_O(X-1)}{T_4(1-Y)} \tag{35}$$

respectively. The performance characteristic curves of the SOFC−GT hybrid system are shown by curve 3 in Figures 11 and 12.

When there is not a regenerator in the GT,[56] $K_R = 0$, $\delta_r = 0$, and the power density and efficiency of the hybrid system

$$P = -\frac{A_c \Delta h}{n_e F}\left\{i\eta_e + \left[1 - \frac{T_{4,\eta}Y - T_O}{T_{4,\eta} - T_O X}\right][(1-\eta_e)i - a_2(T - T_O)]\right\} \tag{36}$$

and

$$\eta = \eta_e + \left[1 - \frac{T_{4,\eta}Y - T_O}{T_{4,\eta} - T_O X}\right]\left[1 - \eta_e - \frac{a_2}{i}(T - T_O)\right] \tag{37}$$

can be obtained from eqs 28 and 29, respectively. Equations 30 and 31 can be simplified as

$$q_1 = A_H K_H (T_4 - T_O X)/\ln\left(\frac{T - T_O X}{T - T_4}\right) \tag{38}$$

and

$$\eta_h = 1 - \frac{T_4 Y - T_O}{T_4 - T_O X} \tag{39}$$

respectively. The performance characteristic curves of the SOFC−GT hybrid system are shown by curve 5 in Figures 11 and 12.

4.3. Case of $c_p \to \infty$. When $c_p \to \infty$, the isobaric processes in the heat engine will become isothermal processes. In this case, $T_{2S} = T_2 = T_3 = T_4$, $T_1 = T_5 = T_6$, $\delta_c = \delta_e = 1$, $\delta_r = 0$, and the working substance cycle in the heat engine becomes the Carnot cycle consisting of two isothermal and two reversible adiabatic processes. The efficiency and heat input rate of the Carnot heat engine can be expressed as

$$\eta_C = 1 - \frac{T_1}{T_4} \tag{40}$$

and

$$q_1 = \frac{AK_H T_4 (T - T_4)(T_1 - T_O)}{K_H T_1 (T - T_4)/K_L + T_4 (T_1 - T_O)} \tag{41}$$

respectively, where $A = A_H + A_L$. The power output and efficiency of the hybrid system can be simplified as

$$P = -\frac{A_c \Delta h}{n_e F}\left\{i\eta_e + \left(1 - \frac{T_{1,\eta}}{T_{4,\eta}}\right)[(1-\eta_e)i - a_2(T - T_O)]\right\} \tag{42}$$

and

$$\eta = \eta_e + \left(1 - \frac{T_{1,\eta}}{T_{4,\eta}}\right)\left[1 - \eta_e - \frac{a_2}{i}(T - T_O)\right] \tag{43}$$

respectively, where $T_{1,\eta}$ and $T_{4,\eta}$ are determined by using the similar method mentioned above. The performance characteristic curves of the SOFC−Carnot cycle hybrid system can be shown by curve 2 in Figures 11 and 12.

If $K_H = K_L \to \infty$, the irreversible losses of heat transfer between the Carnot heat engine and the heat reservoirs are negligible, $T_{2S} = T_2 = T_3 = T_4 = T$, $T_1 = T_6 = T_5 = T_O$, and the Carnot heat engine in the SOFC-based hybrid system becomes a reversible one.[20,57] The power output and efficiency of the hybrid system can be simplified as

$$P = -\frac{A_c \Delta h}{n_e F}\left\{i\eta_e + \left(1 - \frac{T_O}{T}\right)[(1-\eta_e)i - a_2(T - T_O)]\right\} \tag{44}$$

and

$$\eta = \eta_e + \left(1 - \frac{T_O}{T}\right)\left[1 - \eta_e - \frac{a_2}{i}(T - T_O)\right] \tag{45}$$

respectively. The performance characteristic curves of the hybrid system can be shown by curve 1 in Figures 11 and 12.

5. CONCLUSIONS

A generic hybrid system composed of a solid oxide fuel cell and a heat engine is established, in which the waste heat can be effectively utilized. On the basis of the models of the solid oxide fuel cell and Brayton cycle with a regenerative process, expressions for the power output and efficiency of the hybrid system are derived. The optimally operating regions of the power density, efficiency, and current density are determined. The performance characteristics of not only a solid oxide fuel cell−Brayton heat engine hybrid system but also solid oxide fuel cell−gas turbine and solid oxide fuel cell−Carnot heat engine hybrid systems can be directly revealed. The influence of the regenerative process in the heat engine on the performance of the hybrid system is discussed in detail. The results obtained

dx.doi.org/10.1021/ef300839m | Energy Fuels 2012, 26, 5177−5185

here may provide some help for further understanding the optimum design and operation of practical solid oxide fuel cell-based hybrid systems.

AUTHOR INFORMATION

Corresponding Author

*E-mail: jcchen@xmu.edu.cn. Fax: 0086 592 2189426. Tel.: 0086 592 2180922.

Notes

The authors declare no competing financial interest.

ACKNOWLEDGMENTS

This work has been supported by the National Natural Science Foundation (No. 51076134) and the Fundamental Research Fund for the Central Universities (No. 201112G007), People's Republic of China.

NOMENCLATURE

P_e = power output of SOFC
P_h = power output of heat engine
P = power output of hybrid system
η_e = efficiency of SOFC
η_h = efficiency of heat engine
η = efficiency of hybrid system
P^* = power density
Z = product of efficiency and power output
q_1, q_2, q_R, q_L = rate of heat flow
E = open voltage of SOFC
V_{act} = activation overpotential
V_{ohm} = ohmic overpotential
V_{con} = concentration overpotential
ΔH = total enthalpy change
$\Delta h(T)$ = molar enthaply change
$\Delta g(T)$ = molar Gibbs free energy change
T = temperature of SOFC
T_O = temperature of environment
p_0 = pressure of SOFC
p_{H_2} = partial pressure of H_2
p_{O_2} = partial pressure of O_2
p_{H_2O} = partial pressure of H_2O
i = current density
$i_{o,a}$ = anode exchange current density
$i_{o,c}$ = cathode exchange current density
$i_{L,a}$ = anode limiting current density
$i_{L,c}$ = cathode limiting current density
A_c = area of the interconnect plate of SOFC
A, A_H, A_L, A_l, A_R = heat transfer area
K_H, K_L, K_l, K_R = heat transfer coefficient
n_e = number of electrons
F = Faraday's constant
R = universal gas constant
L_{el} = thickness of electrolyte
E_{el} = activation energy for ion transport
σ_0 = reference ionic conductivity
δ_c = compression efficiency
δ_e = expansion efficiency
δ_r = regeneration efficiency
r_p = pressure ratio
γ = ratio of specific heats
$\dot{m}$ = mass flow rate
c_p = specific heat at constant pressure

REFERENCES

(1) Leucht, F.; Bessler, W. G.; Kallo, J.; Friedrich, K. A.; Muller-Steinhagen, H. J. *Power Sources* **2011**, *196*, 1205−15.
(2) Li, Y.; Weng, Y. J. *Power Sources* **2011**, *196*, 3824−35.
(3) Xu, X.; Xiao, Y.; Qiao, C. *Energy Fuels* **2007**, *21*, 1688−94.
(4) Chung, T.; Chyou, Y.; Hong, W.; Cheng, Y.; Lin, K. *Energy Fuels* **2007**, *21*, 314−21.
(5) Calise, F.; Palombo, A.; Vanoli, L. J. *Power Sources* **2006**, *158*, 225−44.
(6) Veyo, S. E.; Shockling, L. A.; Dederer, J. T.; Gillett, J. E.; Lundberg, W. L. *J. Eng. Gas Turbines Power* **2002**, *124*, 845−9.
(7) Costamagna, P.; Magistri, L.; Massardo, A. F. J. *Power Sources* **2001**, *96*, 352−68.
(8) Kaneko, T.; Brouwer, J.; Samuelsen, G. S. J. *Power Sources* **2006**, *160*, 316−25.
(9) Wu, X. J.; Huang, Q.; Zhu, X. J.; Int., J. *Hydrogen Energy* **2011**, *36*, 885−92.
(10) Cheddie, D. F.; Int., J. *Hydrogen Energy* **2011**, *36*, 1702−9.
(11) Wu, X. J.; Huang, Q.; Zhu, X. J. J. *Power Sources* **2011**, *196*, 1295−320.
(12) Bao, C.; Cai, N.; Croiset, E. J. *Power Sources* **2011**, *196*, 8424−34.
(13) Wu, X. J.; Zhu, X. J. J. *Power Sources* **2011**, *196*, 8444−9.
(14) Burbank, W., Jr.; Witmer, D.; Holcomb, F. J. *Power Sources* **2009**, *193*, 656−64.
(15) Bang-Moller, C.; Rokni, M.; Elmegaard, B. *Energy* **2011**, *36*, 4740−52.
(16) Cocco, D.; Tola, V. *Energy Convers. Manage.* **2009**, *50*, 1040−8.
(17) Zhang, X. W.; Chan, S. H.; Li, G. J.; Ho, H. K.; Li, J.; Feng, Z. P. J. *Power Sources* **2010**, *195*, 685−702.
(18) Roberts, R.; Brouwer, J.; Jabbari, F.; Junker, T.; Ghezel-Ayagh, H. J. *Power Sources* **2006**, *161*, 484−91.
(19) Cheddie, D. F.; Murray, R. J. *Power Sources* **2010**, *195*, 8134−40.
(20) Haynes, C. J. *Power Sources* **2001**, *92*, 199−203.
(21) Zhang, X.; Su, S.; Chen, J.; Zhao, Y.; Brandon, N. *Int. J. Hydrogen Energy* **2011**, *36*, 15304−12.
(22) Winkler, W.; Lorenz, H. J. *Power Sources* **2002**, *106*, 338−43.
(23) Zhang, X.; Chen, J. *Int. J. Hydrogen Energy* **2010**, *35*, 284−93.
(24) Costamagna, P.; Honegger, K. J. *Electrochem. Soc.* **1998**, *145*, 3995−4007.
(25) Noren, D. A.; Hoffman, M. A. J. *Power Sources* **2005**, *152*, 175−81.
(26) Ji, Y.; Yuan, K.; Chung, J. N.; Chen, Y. C. J. *Power Sources* **2006**, *161*, 380−91.
(27) Zhu, H.; Kee, R. J. J. *Power Sources* **2003**, *117*, 61−74.
(28) Akkaya, A. V. *Int. J. Energy Res.* **2007**, *31*, 79−98.
(29) Larminie, J.; Dicks, A. *Fuel Cell Systems Explained*, Second ed.; Wiley: New York, 2003.
(30) Musa, A.; De Paepe, M. *Int. J. Hydrogen Energy* **2008**, *33*, 4665−72.
(31) Zhang, Y.; Hu, W.; Ou, C.; Chen, J. *Appl. Therm. Eng.* **2009**, *29*, 1766−72.
(32) Sánchez-Orgaz, S.; Medina, A.; Calvo Hernández, A. *Energy Convers. Manage.* **2010**, *51*, 2134−43.
(33) Zhang, Y.; Ou, C.; Lin, B.; Chen, J. J. *Energy Res. Technol.* **2006**, *128*, 216−22.
(34) Bejan, A. *Advanced engineering thermodynamics*; Wiley: New York, 1988.
(35) Chen, J. *J. Phys. D: Appl. Phys.* **1994**, *27*, 1144−9.
(36) Sánchez, D.; Chacartegui, R.; Muñoz, A.; Sánchez, T. J. *Power Sources* **2006**, *160*, 1074−87.
(37) Bavarsad, P. G. *Int. J. Hydrogen Energy* **2007**, *32*, 4591−9.
(38) Chen, J.; Andresen, B. *Heat Recovery Syst. CHP* **1995**, *15*, 723−31.
(39) Sánchez, D.; Muñoz, A.; Sánchez, T. J. *Power Sources* **2007**, *169*, 25−34.
(40) Shin, Y.; Park, W.; Chang, J.; Park, J.; Int., J. *Hydrogen Energy* **2007**, *32*, 1486−91.

(41) Dean, J. A. *Lange's Handbook of Chemistry*, 13th ed.; McGraw Hill Book Company: New York, 1985.
(42) Yoon, K. J.; Zink, P.; Gopalan, S.; Pal, U. B. J. *Power Sources* **2007**, *172*, 39−49.
(43) Costamagna, P.; Selimovic, A.; Del Borghi, M.; Agnew, G. *Chem. Eng. J.* **2004**, *102*, 61−9.
(44) Zhu, H.; Kee, R. J.; Janardhanan, V. M.; Deutschmann, O.; Goodwin, D. G. J. *Electrochem. Soc.* **2005**, *152*, A2427−40.
(45) Cheddie, D.; Murray, R. *Int. J. Hydrogen Energy* **2010**, *35*, 11208−15.
(46) Park, S. K.; Ahn, J.; Kim, T. S. *Appl. Energy* **2011**, *88*, 2976−87.
(47) Cardu, M.; Baica, M. *Energy Conver. Manage.* **1999**, *40*, 71−87.
(48) Lora, E. E. S.; Salomon, K. R. *Energy Conver. Manage.* **2005**, *46*, 1293−303.
(49) Villela, I. A. C.; Silveira, J. L. *Appl. Therm. Eng.* **2007**, *27*, 840−7.
(50) Subramanyan, K.; Diwekar, U.; Goyal, A. J. *Power Sources* **2004**, *132*, 99−112.
(51) Haseli, Y.; Dincer, I.; Naterer, G. F.; Int., J. *Hydrogen Energy* **2008**, *33*, 5811−22.
(52) Yang, W. J.; Park, S. K.; Kim, T. S.; Kim, J. H.; Sohn, J. L.; Ro, S. T. J. *Power Sources* **2006**, *160*, 462−73.
(53) Le Roux, W. G.; Bello-Ochende, T.; Meyer, J. P. *Energy* **2011**, *36*, 6027−36.
(54) Jubeh, N. M. *Entropy* **2005**, *7*, 172−87.
(55) Sánchez, D.; Muñoz de Escalona, J. M.; Chacartegui, R.; Muñoz, A.; Sánchez, T. J. *Power Sources* **2011**, *196*, 4347−54.
(56) Aguiar, P.; Brett, D. J. L.; Brandon, N. P.; Int., J. *Hydrogen Energy* **2008**, *33*, 7214−23.
(57) Ro, S. T.; Sohn, J. L. J. *Power Sources* **2007**, *167*, 295−301.